UNSYS digital

International Journal of Robotics and Mechatronics

A Parametric Study on the Sub-surface Stresses in Spur Gears under Mixed-lubrication Regime using Load-sharing and Finite Element Simulation

Mohammad Danesh, Saleh Akbarzadeh, Peiman Mosaddegh, Morteza Parsa

Department of Mechanical Engineering, Isfahan University of Technology, Isfahan, Iran

***Abstract*—**Gears as key elements in power transmission systems are widely used in industry. Based on the manufacturing process, the surface of gears compared to other mechanical components such as roller bearings might be rougher and thus the effect of surface roughness in their performance should be given full consideration. One of the most important parameters in the gears' performance is the maximum shear stress that occurs below the surface, which is believed to be the key factor in surface fatigue and pitting. In this research, a model that employs the load-sharing concept to predict the friction coefficient and film thickness for each point along the line of action is developed. The sub-surface stress field that is generated below the tooth surface is calculated based on the friction coefficient. The predicted sub-surface stresses are compared to the results obtained from the commercial finite element software ABAQUS. An acceptable agreement is observed in comparing the results from the two methods. Finally, a parametric study has been conducted to study the effect of load, velocity, viscosity and surface hardness on the calculated maximum sub-surface shear stress and its location.

***Keywords*—**Sub-surface stresses, ABAQUS, spur gear, load-sharing concept, finite element simulation.

I. Introduction

WHEN When two curved bodies such as wheel and rail trains, cam and follower, gear teeth, and rolling bearings experience contact, surface and sub-surface stresses are induced in the contacting bodies. Rolling contact fatigue theory is based on the assumption that when two surfaces are pressed together, micro cracks are formed and rapidly grown under the effect of shear stresses [1, 2]. If the contact is lubricated, the lubricant is penetrated into the cracks and under high pressures, separates the loose pieces. To predict the possibility of failure in these cases, it is necessary to examine the state of stress due to the loading conditions between two counterpart bodies [2].

Gears are widely used in various power transmission systems. To guarantee the optimum life of the gears, the sub-surface stresses below a certain level should be considered in the design. In many cases, the first visible sign of the surface failure is the wear mark that can be observed near the pitch line. It is postulated that these wear marks are produced as a result of high sub-surface shear stresses. Thus, the ability to predict the value of the sub-surface stresses and the depth in which it occurs enables the designer to perform a better evaluation on the type of possible surface failures and taking measures to prevent them [2]. For instance, one can choose the suitable anti-wear coating thickness for the surface to prevent occurrence of the cracks. With the changes in material, lubricants, surface hardness, surface quality, transmitted load, and speed, it is possible to control the maximum shear stress induced below the surface, which in turn leads to surface fatigue and pitting [3].

Study of the surface and sub-surface stresses in contacting bodies is investigated for a decade. Kannel and Tevaarwerk studied the sub-surface stresses in sliding-rolling contacts by using the stress tensor at each point below the surface [1]. The sub-surface stress field for dry rectangular contact has been examined by Mihailidis *et al*. [4]. They numerically generated the surface roughness of the two cylinders and evaluated the effect of surface roughness on the surface and sub-surface stresses. Their results showed that the maximum stress occurs at relatively small depth below the surface. They have also claimed that this stress is greater than the stress which is predicted using the Hertzian stress formulation.

Majumdar and Hamrock [5] and Patir and Cheng [6] conducted researches on the effect of surface roughness on the elastohydrodynamic line contact problem. Greenwood *et al*. [7] introduced roughness parameter in the Hertzian contact problem. They proposed correction factors to modify the stress obtained from the Hertz theory.

Since the gears usually operate under the mixed lubrication regime, the asperities contribute in carrying the load. One powerful method to address this type of problems is the load-sharing concept in which it is assumed that the total transmitted load is carried by the lubricant film as well as the contact of asperities [8]. Gelinck and Schipper [9] extended this concept to the line contact problem. Lu *et al*. [10] used this method to predict the friction coefficient in heavily-loaded journal bearings. Akbarzadeh and Khonsari [11,12] employed the load-sharing concept to the isothermal as well as the thermal analysis of spur gears. Ebrahimi Serest and

Corresponding author: Peiman Mosaddegh (e-mail: mosadegh@cc.iut.ac.ir).
This paper was submitted on December 11, 2013; revised on December 12, 2014; and accepted on December 22, 2014.

Akbarzadeh [13] developed this model to the contact of helical gears and Bahrami Ghahnavieh *et al*. [14] extended this analysis to the straight bevel gears. Masjedi and Khonsari [15] developed curvefits to predict the contribution of asperities and film thickness in the mixed-lubrication line contact problems. Later they conducted experiments to measure the friction coefficient in the mixed-lubricated line contact problems [16].

In this study, the contact of pinion and gear at any point along the line of action is replaced by the contact of two cylinders. The radii of these cylinders as well as the applied load change along the line of action. Employing the load-sharing concept developed by Johnson *et al*. [8] and the contact model developed by Zhao *et al*. [17], the performance parameters such as central film thickness, the load carried by the asperities, the load carried by the lubricant film, and friction coefficient corresponding to each point along the line of action are obtained. The calculated friction coefficient is then used in the formulation of sub-surface stresses. To verify the results, sub-surface stresses are simulated using the commercial finite element software ABAQUS and compared to the results obtained in this paper. Finally, a parametric study has been conducted, which evaluates the effect of load, speed, lubricant's viscosity, and material's hardness on the calculated maximum sub-surface stress and its location. The presented work has a short execution time and an acceptable accuracy compared to other researches in this field.

II. Modeling

The modeling section starts with an introduction to the load-sharing concept and continues with formulation of the sub-surface stresses that are formed due to the load that is transmitted by the gear teeth.

A. Load-Sharing Concept

The contact of spur gears is usually in the mixed-lubrication regime in which both the asperities and the lubricant film contribute in carrying the load [8]. Contact of a pair of spur gears at an arbitrary point along the line of action which is replaced by contact of a pair of cylinders is illustrated in Figure 1. The mean height of the surfaces as well as the contact of the asperities is schematically shown in this figure.

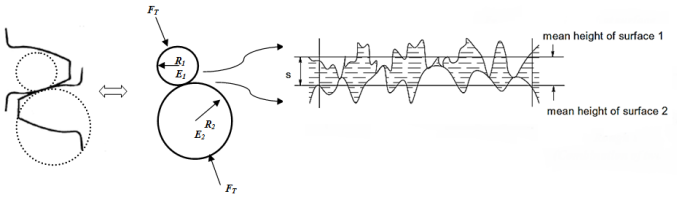

Figure 1 Contact of a pair of spur gears at an arbitrary point

Based on the load-sharing concept, a part of the total applied force, F_T, is carried by the lubricant film, F_H, and the rest of the load is carried by asperities, F_c [8]:

$$F_T = F_H + F_C \tag{1}$$

Similarly, the friction force, F_f , is divided into two parts; the first component of friction force, $F_{f,c}$, which is due to the contact between the surface asperities and the second component, $F_{f,H}$, is because of the shearing of the lubricant film. The friction coefficient, *f*, is obtained using the following formulas:

$$f = \frac{F_f}{F_T} \tag{2}$$

$$F_f = F_{f,C} + F_{f,H} \tag{3}$$

$$F_{f,C} = \sum_{i=1}^{N} \iint_{A_{Ci}} \tau_{Ci}\, dA_{Ci} = f_c\, F_C \tag{4}$$

$$F_{f.H} = \frac{U_{dif}\eta}{s} \times A_H = \tau_H A_H \tag{5}$$

Where η (Pa.s) is the dynamic viscosity, U_{dif} (m/s) is the sliding speed of the contacting surfaces, *S* (m) is the local separation between the surfaces, f_c is the asperities friction coefficient, A_C is the real area of contact, and A_H is the lubricant film contact area.

The scaling factors, γ_1 and γ_2, are defined as [8]:

$$\frac{F_H}{F_T} + \frac{F_C}{F_T} = \frac{1}{\gamma_1} + \frac{1}{\gamma_2} = 1 \tag{6}$$

Where γ_1 is lubricant film scaling factor and γ_2 is the asperities scaling factor. The central film thickness is calculated using the modified Moes equation [18].

$$H_C = \left[\gamma_1^s \left(H_{RI}^{7/3} + H_{EI}^{7/3} \right)^{3s/7} + \left(H_{RP}^{-7/2} + H_{EP}^{-7/2} \right)^{-2s/7} \right]^{1/s} \tag{7}$$

$$s = 1/5 \left(7 + 8e^{\left(-2 H_{EI}\, \gamma_1^{-2/5} / H_{RI} \right)} \right) \tag{8}$$

Where H_{RI}, H_{EI}, H_{EP}, and H_{RP} are dimensionless numbers, which are defined as follows.

$$W = \frac{F_T}{E' RB} \tag{9}$$

$$U_\Sigma = \frac{\eta_0 u_s}{E' R} \tag{10}$$

$$M = W U_\Sigma^{-.05} \tag{11}$$

$$G = \alpha E' \tag{12}$$

$$L = G U_\Sigma^{-0.5} \tag{13}$$

$$H_{RI} = 3M^{-1} \quad (14)$$

$$H_{EI} = 2.621M^{-1/5} \quad (15)$$

$$H_{EP} = 1.311M^{-1/8}L^{3/4} \quad (16)$$

$$H_{RP} = 1.287L^{2/3} \quad (17)$$

$$H_C = h_C^{'}U_{\Sigma}^{-0.5} \quad (18)$$

$$h_C^{'} = \frac{h_C}{R} \quad (19)$$

In the above relations B is the cylinder's width, $E^{'}$ is the equivalent Young's modulus of pinion and gear, R is the equivalent radius of curvature of the cylinders, α is the lubricant's pressure-viscosity factor, H_C is the dimensionless film thickness, L and G are dimensionless lubricant parameter, M and W are dimensionless load, U_{Σ} is the dimensionless speed, and h_c is the central thickness of the lubricant film.

As a result of contact of asperities, each asperity i experience an indentation which is denoted as w_i [8]:

$$w_i = Z_i - d_e \quad (20)$$

The distance between the mean plane of the summits and the rigid flat surface is denoted by d_e as shown in Figure 2 [8].

$$d_e = 0.7h_C \quad (21)$$

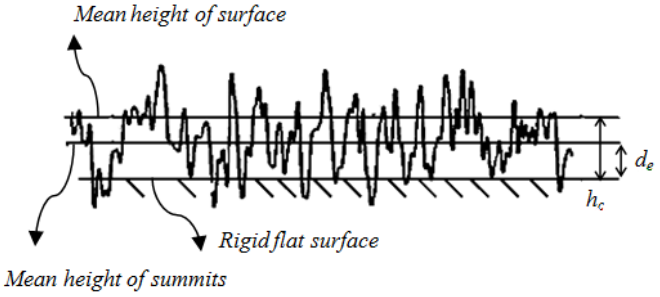

Figure 2 The contact between a rough surface and a rigid flat surface.

The limit for the elastic indentation of a deformed asperity is calculated using the following relation [19].

$$W_e = 0.94\left(H/E^{'}\right)^2\beta \quad (22)$$

Where H is the hardness of the material and β is the average radius of the asperities. When the indentation of the asperity is more than the critical indentation which is calculated in Equation 22, elasto-plastic deformation occurs. If the indentation increases even more, full plastic deformation occurs. The full plastic deformation occurs when the indentation of an asperity reaches 54 times the elastic indentation limit [20].

$$W_P \cong 54W_e \quad (23)$$

Therefore, there is a wide range of elasto-plastic regime between the elastic regime and plastic regime. To calculate the force carried by the asperities in the three distinct regimes, following relations are used [17]:

$$F_{ie}(W_i) = 4/3E^{'}\beta^{0.5}W_i^{1.5} \quad (24)$$

$$F_{ieP}(W_i) = \left(H - 0.6H\frac{\ln W_P - \ln W_i}{\ln W_P - \ln W_e}\right) \times \left(\pi\beta W_i\left(1 - 2\left(\frac{W_i - W_e}{W_P - W_e}\right)^3 + \left(\frac{W_i - W_e}{W_P - W_e}\right)^2\right)\right) \quad (25)$$

$$F_{iP}(W_i) = 2\pi\beta WH \quad (26)$$

Where F_{ie} is the force carried by asperity *i* due to the elastic deformation of the asperity, F_{ieP} is the force carried by asperity *i* due to the elasto-plastic deformation of asperity and F_{iP} is the force carried by asperity *i* due to the plastic deformation of asperity. The total load carried by asperities is obtained by summing all of the components:

$$F_C = \sum F_i(W_i) \quad (27)$$

B. Sub-surface Stresses

During the contact of two cylinders, the shear stresses below the surface can be obtained assuming Hertzian contact relation as shown in **Figure 3** [20]. In this case, the shear stress can be calculated by:

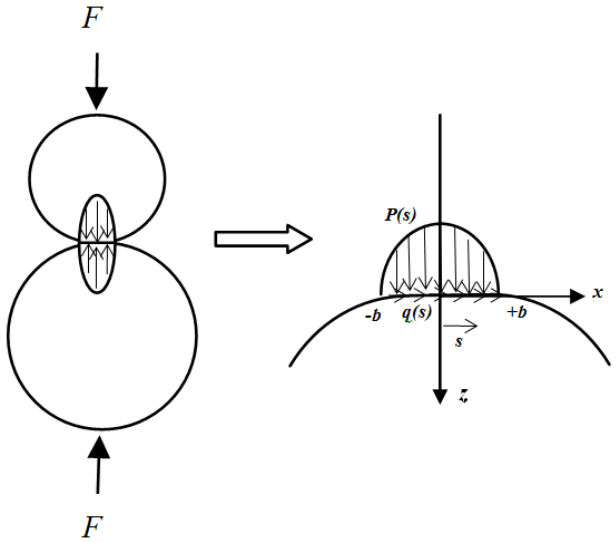

Figure 3 Pressure distribution along the Hertzian width

$$\tau_{xz} = \frac{-2z^2}{\pi}\int_{-b}^{+b}\frac{P(s)(x-s)}{\left[(x-s)^2+z^2\right]^2}ds - \frac{2z}{\pi}\int_{-b}^{+b}\frac{q(s)(x-s)^2}{\left[(x-s)^2+z^2\right]^2}ds \quad (28)$$

$$P(s) = P_{\max}\sqrt{1-\left(s^2/b^2\right)} \tag{29}$$

$$q(s) = f \times P(s) \tag{30}$$

$$P_{\max} = \frac{2F_T}{\pi bB} \tag{31}$$

Where τ_{xz} is the shear stress, f is the friction coefficient, b is the half-width of the Hertzian contact, B is the cylinder's width, F_T is the applied load, and $P_{\max}$ is the Hertzian maximum pressure.

III. Numerical Simulation Procedure Based on Developed Model

First, the load-sharing concept is employed to calculate the friction coefficient for each point along the line of action. Parameters such as pinion and gear's geometry, surface roughness and mechanical properties of pinion and gear as well as lubricant properties are required to calculate the coefficient of friction. These properties are given in **Table I** and **Table II**. The reported roughness data which corresponds to a pair of ground rollers has been used as an input to this model. The obtained friction coefficient is then used in the algorithm for calculating the sub-surface stresses as illustrated in **Figure 4**.

Table I Surface Properties [21]

Parameters	Value	Unit	Definition
R_a	0.7534	µm	The average arithmetic of asperities height
R_q	0.9317	µm	Standard deviation of asperities height
R_t	4.3152	µm	Peak height to maximum valley
β	10.932	µm	The average radius of the asperities
N	10^9*4.0173	$1/m^2$	Density of asperities
f_C	0.1	-	Friction coefficient between the asperities

Table II Gear and Lubricant Properties [21]

Parameters	Value	Unit	Definition
z_P	21	-	Pinion tooth number
z_g	32	-	Gear tooth number
M	0.003	m	Modulus
d_{wp}	0.063	m	Pitch diameter of pinion
ω	1515	rpm	Angular velocity of pinion
B	0.16	m	Gear width
F	125000	N/m	Load per gear width
α	20	Deg	Pressure angle
η_0	0.065	Pa. s	Viscosity at atmospheric pressure
Z	0.6	-	Exponent of viscosity-pressure relationship
E'	219.78	GPa	Equivalent Young modulus
H	1	GPa	Hardness

The above formulation has been implemented in Matlab software and the location and the value of the maximum shear stress are shown in **Table III**. The shear stress contour for the contact of a rigid smooth surface with a rough cylinder is plotted in **Figure 5** for the first point of line of action.

Table III The location and value of the maximum shear stress

S_{zx_Max} (MPa)	Z_{Max}(m)	X_{Max}(m)
60.95	1.328 e-004	-8.418 e-005

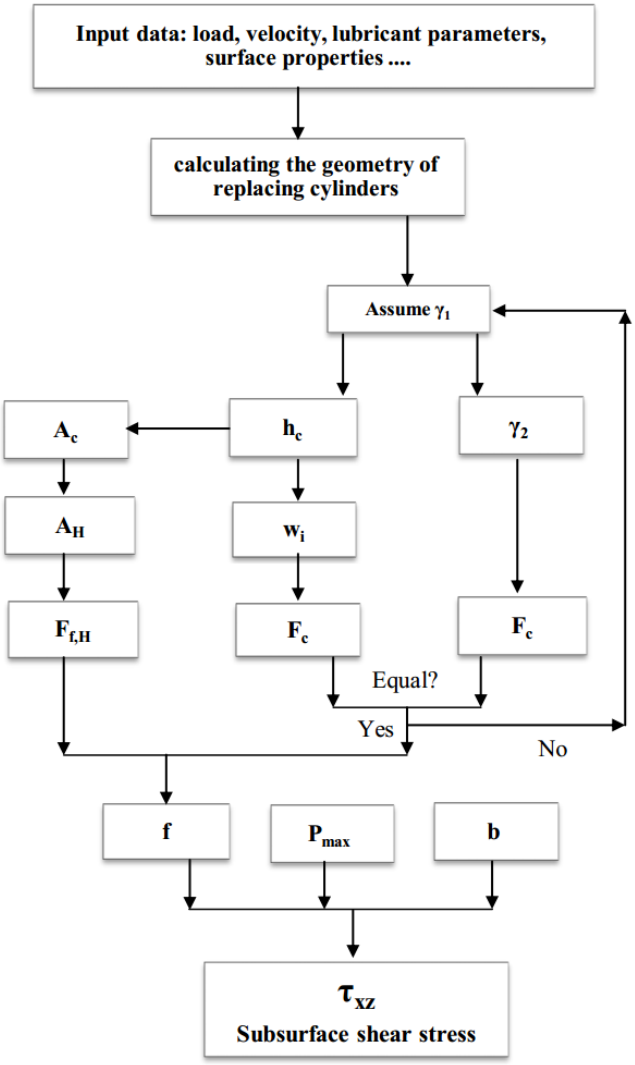

Figure 4 The flowchart to obtain sub-surface shear stress

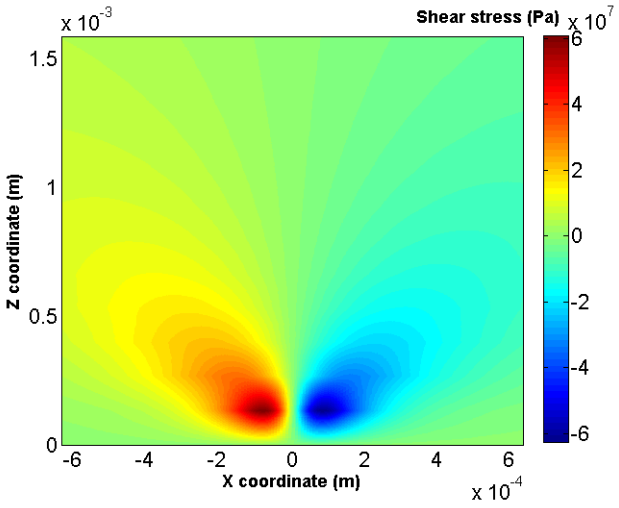

Figure 5 Shear stress contour (Pa) of the contact of the rigid smooth surface with a rough cylinder

IV. FINITE ELEMENT SIMULATION PROCEDURE

In this section, the contact of two cylinders which represent the contact in the first point of the line of action is simulated using the commercial finite element software, ABAQUS and illustrated in **Figure 6**. This geometrical transformation reduces computational time since modeling of the contact of actual profile of pinion and gear requires fine meshes close to the contact zone. Inputs required by ABAQUS software, such as modulus of elasticity, applied load, and friction coefficient are similar to the real gear contact and are reported in **TABLE IV**. These data are obtained from the load-sharing analysis. As explained earlier, the effect of asperities is considered in the friction coefficient which is used in the finite element simulation.

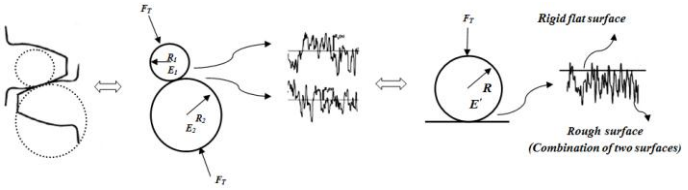

Figure 6 The process of replacing the contact of the pinion and gear with the contact of cylinder and the rigid smooth surface

TABLE IV THE INPUTS NEEDED TO MODEL THE CONTACT OF RIGID SMOOTH SURFACE WITH ROUGH CYLINDER

Parameters	Value	Unit	Definition
F	6666.7	N	Applied force
f	0.0209	-	Friction coefficient
$E^{'}$	219.78	GPa	Equivalence Young Modulus
R	0.0032871	m	Equivalent radius of curvature of cylinder

The loading and boundary conditions in ABAQUS modeling are shown in **Figure 7**. A concentrated force is applied in point A, the point B is fix in X direction and point C reference point of rigid surface, is fixed in X and Y direction.

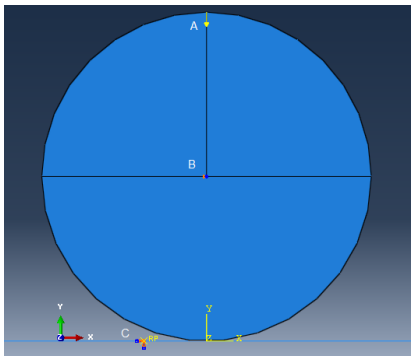

Figure 7 Loading and boundary conditions

In ABAQUS software, the plain strain mesh type with quad-free-advanced mesh structure is used. Because of the complicated type of contact and small value of the equivalent radius of curvature of cylinders, the mesh size should be very fine as depicted in **Figure 8**. In order to evaluate the convergence of results, sensitivity analysis of the mesh size has been done in FE analysis and the results are shown in **Figure 9**.

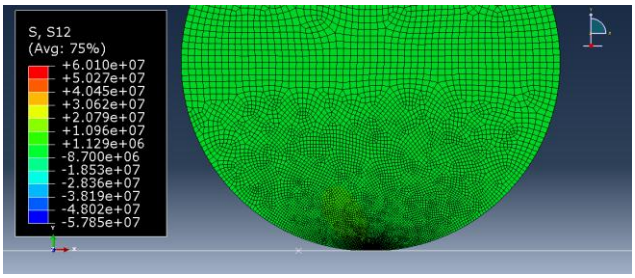

Figure 8 Contact of the rigid smooth surface with rough cylinder with the distribution of meshing.

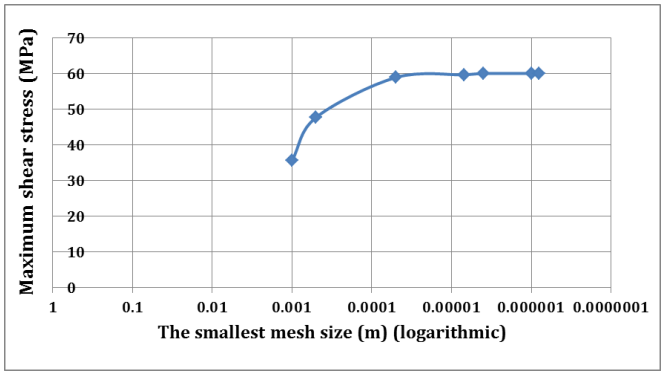

Figure 9 Mesh convergence analysis results

The small difference in the shear stresses at the contact between the two cylinders and contact between the real gear teeth is due to the differences in the amount of contact width. However, at the point of contact both cases have equal curvature, but for the other points near the contact point, the gear tooth profile curvature is different from the cylindrical one with equivalent radius of curvature. Shear stress contour obtained from ABAQUS software for the contact of rigid smooth surface with rough cylinders are shown in **Figure 10**.

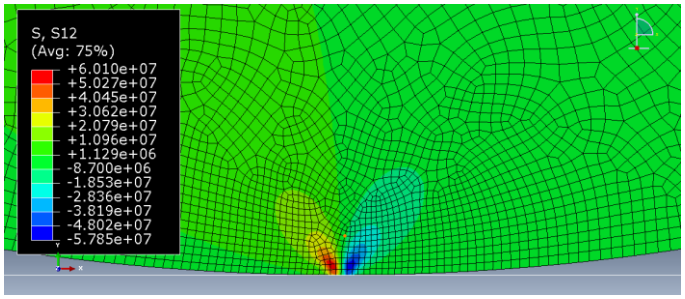

Figure 10 Shear stress contour of the contact of the rigid smooth surface with rough cylinder by ABAQUS

V. Results and Discussion

Results obtained from the finite element method and the results obtained from the load-sharing concept are illustrated in **Table V** and **Figure 10**, respectively. The two sets of results are fairly close.

Table V The comparison of the maximum shear stress obtained from the load-sharing concept and the finite element method

Maximum Shear Stress by load-sharing concept	Maximum Shear Stress by Finite element method	Percentage of error
60.95 MPa	60.10 MPa	1.414 %

In this section, the effect of load, velocity, lubricant viscosity, and surface hardness on the maximum shear stress and its location has been studied.

A. *Effect of load*

The effect of applied load, F_T, on the maximum shear stress and its location is shown in **Figures 11** and **12**, respectively. As seen in Equations 28 to 31, by increasing the amount of load, the maximum shear stress increases and its location moves inside the material.

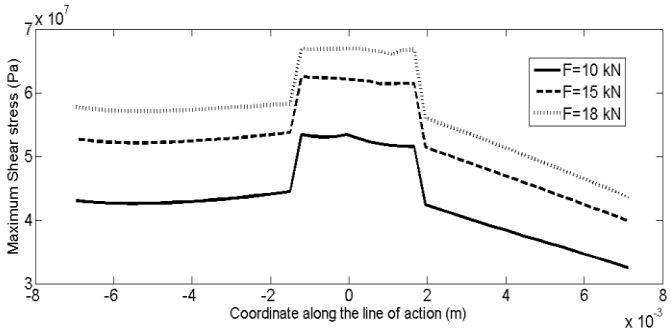

Figure 11 Effect of load on the maximum shear stress

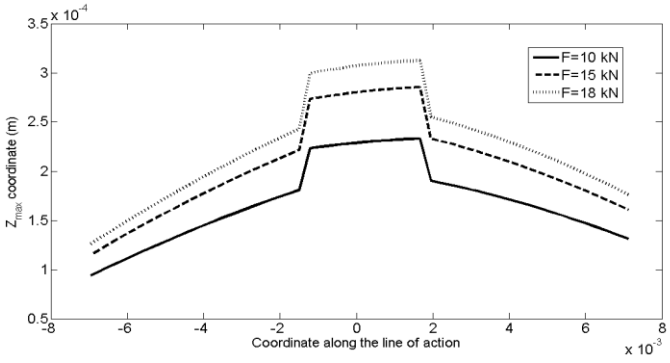

Figure 12 Effect of load on the location of maximum shear stress

B. *Effect of velocity*

The effect of velocity on the maximum shear stress and its location is shown in **Figures 13** and **14**, respectively. Increasing the velocity results in decreasing of friction

coefficient, *f*, and the total load carried by asperities, $F_{f,c}$. Due to the linear relation between the friction coefficient and the sub-surface shear stress, as the velocity increases the maximum shear stress decreases and its location coordinate moves toward the surface of the gear.

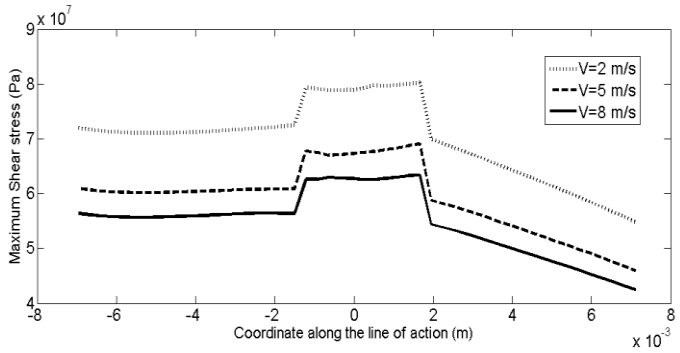

Figure 13 Effect of velocity on the maximum shear stress

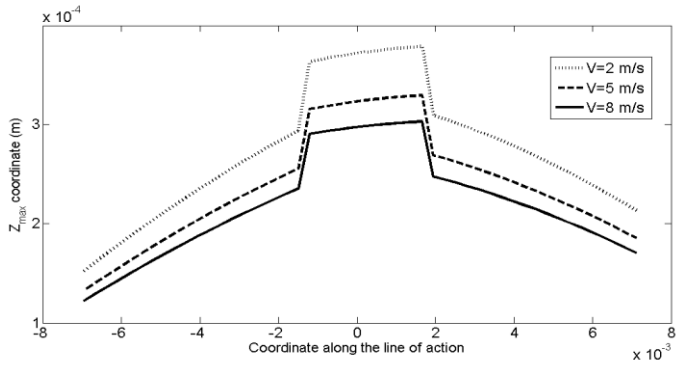

Figure 14 Effect of velocity on the location of maximum shear stress

C. *Effect of Lubricant's viscosity*

The effect of viscosity on the maximum shear stress and its location is shown in **Figures 15** and **16**, respectively. By increasing the viscosity, the load carried by the lubricant increases, therefore the total load carried by asperities decreases. Therefore' maximum shear stress decreases and its location coordinate moves toward the surface as shown in **Figure 15**.

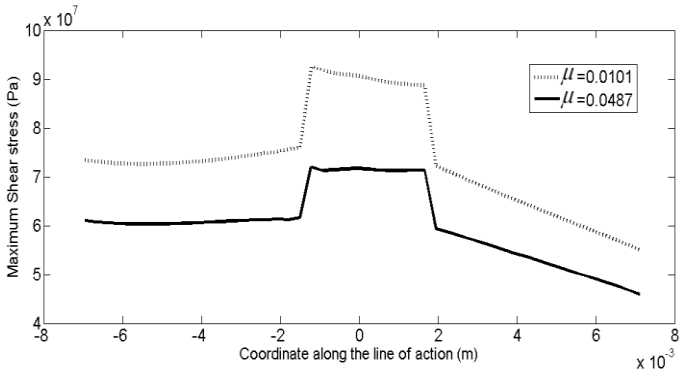

Figure 15 Effect of viscosity on the maximum shear stress

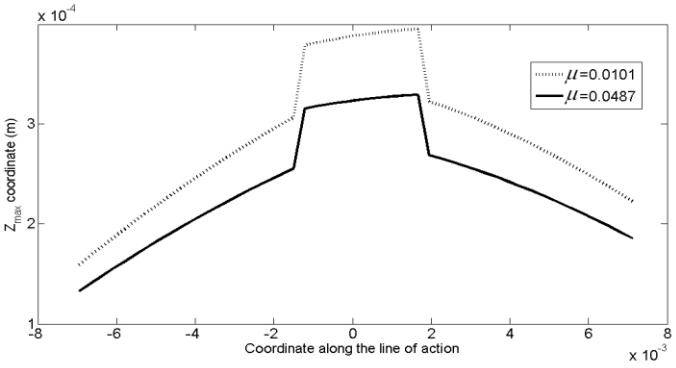

Figure 16 Effect of viscosity on the location of maximum shear stress

D. *Effect of surface hardness*

The effect of surface hardness on the maximum shear stress and its location is shown in **Figures 17** and **18**, respectively. Increasing the surface hardness results in an increase in the total load carried by asperities, $F_{f,c}$. Therefore, as the hardness increases the maximum shear stress increases and its location coordinates moves toward inside the body as shown in **Figures 17** and **18**.

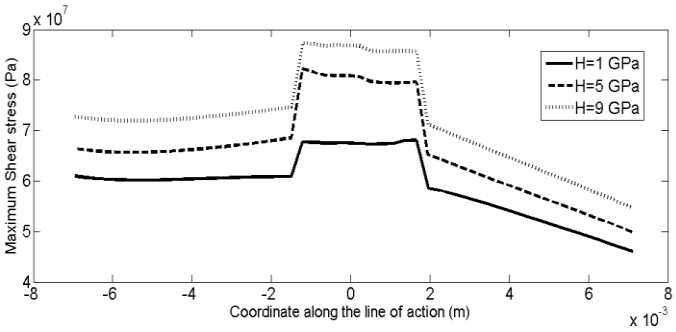

Figure 17 Effect of hardness on the maximum shear stress

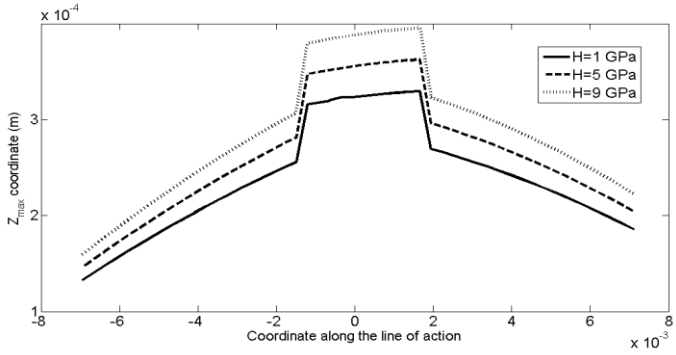

Figure 18 Effect of hardness on the location of maximum shear stress

VI. CONCLUSION

In this study, the location and the amount of the maximum sub-surface shear stress which is believed to be responsible for surface failures such as fatigue is studied. The friction is one of the important parameters affecting the sub-surface stresses. For obtaining the friction coefficient of gear and pinion in contact,

the contact between the gear and pinion is replaced with two cylinders at any point along the line of action. The load-sharing concept is employed to determine the contribution of asperities in carrying the load and the friction coefficient. After obtaining the friction coefficient, the maximum shear stress for any point on the line of action is determined. The results are verified by comparing the obtained results to the finite element simulations using ABAQUS. The parametric study indicates that by increasing the amount of load, the maximum shear stress increases and its location moves inside of the material and as the velocity increases the maximum shear stress decreases and its location coordinate moves toward the surface of the gear. By increasing the amount of viscosity, maximum shear stress decreases and its location coordinate moves toward the surface and as the material hardness increases the maximum shear stress increases and its location coordinates moves toward inside the body.

REFERENCES

[1] Kannel, J.W., and Tevaarwerk, J.L., "Stress Evaluation under Rolling/ Sliding Contacts", NASA CR-165561, Oct. 1981.

[2] Beheshti, A., and Khonsari, M.M., "On the prediction of fatigue crack initiation in rolling/sliding contacts with provision for loading sequence effect", Tribology International, pp. 1620-1628, 2011. CrossRef

[3] Fernandens, P.J.L., and Mcduling, C., "Surface contact fatigue failures in gears", Engineering Failure Analysis. vol. 4, pp. 99–107, 1997. CrossRef

[4] Mihailidis, A., Bakolas, V., and Balkan, J., "Numerical simulation of real 3-D rough surfaces", J. Balkan Tribol. Assoc. 5 pp. 247–255, 1999.

[5] Majumdar, B.C., and Hamrock, B. J., "Effect of Surface-Roughness on Elastohydrodynamic Line Contact", J Lubric. Tech-T ASME. Vol. 104(3), pp. 401-409, 1982. CrossRef

[6] Patir, N., and Cheng, H. S., "An Average Flow Model for Determining Effects of Three-Dimensional Roughness On Partial Hydrodynamic Lubrication", ASME J. Lubr. Technol., Vol. 100, pp. 8–14, 1978. CrossRef

[7] Greenwood, J.A., Johnson, K.L., and Matsubara, E., "A surface roughness parameter in Hertz contact", wear. vol. 100, pp. 47-57, 1984.

[8] Johnson, K.L., Greenwood, J. A., and Poon, S. Y., "A Simple Theory of Asperity Contact in Elastohydrodynamic Lubrication", Wear. vol. 19, pp. 91-108, 1972. CrossRef

[9] Gelinck, E.R.M., and Schipper, D. J., "Calculation of Stribeck Curves for Line Contacts", Tribol. vol. 33, pp. 175–181, 2000. CrossRef

[10] Lu, X., Khonsari, M. M., and Gelinck, E. R. M. , "The Stribeck Curve:Experimental Results and Theoretical Prediction", ASME J. Tribol. vol. 128, pp. 789–794, 2006. CrossRef

[11] Akbarzadeh, S., and Khonsari, M.M., "Performance of Spur Gears Considering Surface Roughness and Shear Thinning Lubricant ", Journal of Tribology. vol. 130(2), p. 021503, 2008. CrossRef

[12] Akbarzadeh, S., and Khonsari, M.M., "Thermoelastohydrodynamic analysis of spur gears with consideration of surface roughness", Tribology Letters. vol. 32, pp. 129–141, 2008. CrossRef

[13] Ebrahimi sererst, A., Akbarzadeh, S., "Mixed Elastohydrodynamic Analysis of Helical Gears Using Load-Sharing Concept," Journal of Engineering Tribology, 228, pp.320-331, 2014.

[14] Bahrami Ghahnavieh, A., Akbarzadeh, S., Mosaddegh, P.,"A Numerical Study on the Performance of Straight Bevel Gears Operating Under Mixed Lubrication Regime," Mechanism and Machine Theory, 75, pp. 27-40, 2014. CrossRef

[15] Masjedi, M., and Khonsari, M. M., "Film Thickness and Asperity Load Formulas for Line-Contact EHL with Provision for Surface Roughness", Journal of Tribology. vol. 134,011503, 2012

[16] Masjedi, M., and Khonsari, M. M., "Theoretical and experimental investigation of traction coefficient in line-contact EHL of rough surfaces", Tribology International . vol. 70, pp.179-189, 2014. CrossRef

[17] Zhao, Y., Maietta, D.M., and Chang, L., "An asperity microcontact model incorporating the transition from elastic deformation to fully plastic flow", Tribology. vol. 122, pp. 86-93, 2000. CrossRef

[18] Moes, H., "Optimum similarity analysis with applications to elastohydrodynamic lubrication", Wear. vol. 159, pp. 57-66, 1992. CrossRef

[19] Greenwood, J.A., and Williamson, J.B.P., "Contact of nominally flat surfaces", Proc. R. Soc., vol. 295, pp.300-319, 1966.

[20] Johnson, K.L., Contact mechanics, Cambridge University Press, UK, 1985. CrossRef

[21] M. Parsa and S. Akbarzadeh, “A new load-sharing-based approach to model mixed-lubrication contact of spur gears,” Proc. Inst. Mech. Eng. Part J J. Eng. Tribol., 2014. CrossRef